A 3D weaving infill pattern for fused filament fabrication

Yuan Yao (yaoyuan@shu.edu.cn)
Shanghai University https://orcid.org/0000-0003-3302-4909
Cheng Ding
Shanghai University
Mohamed Aburaia
University of Applied Sciences Technikum Wien
Maximilian Lackner
University of Applied Sciences Technikum Wien
Lanlan He
Shanghai University

Research Article

Keywords: Additive manufacture, 3D weaving path, Anisotropy strength

Posted Date: June 12th, 2021

DOI: https://doi.org/10.21203/rs.3.rs-295081/v1

Abstract

The Fused Filament Fabrication process is the most used additive manufacturing process due to its simplicity and low operating costs. In this process, a thermoplastic filament is led through an extruder, melted, and applied to a building platform by the axial movements of an automated Cartesian system in such a way that a three-dimensional object is created layer by layer. Compared to other additive manufacturing technologies, the components produced have mechanical limitations and are often not suitable for functional applications.

To reduce the anisotropy of mechanical strength in fused filament fabrication (FFF), this paper proposes a 3D weaving deposit path planning method that utilizes a 5-layer repetitive structure to achieve interlocking and embedding between neighbor slicing planes to improve the mechanical linkage within the layers. The developed algorithm extends the weaving path as an infill pattern to fill different structures and makes this process feasible on a standard three-axis 3D printer. Compared with 3D weaving printed parts by layer-to-layer deposit, the anisotropy of mechanical properties inside layers is significantly reduced to 10.21% and 0.98%.

1. Introduction

Additive manufacturing (AM) technology provides more flexible and rapid ways for the designing and manufacturing of modern industry. The fused filament fabrication (FFF), also called Filament-based Fused Deposition Modeling (FDM), is the main forming method in AM, which extrudes molten material from the nozzle to the printing platform by heating, and lays a layer along a certain path step by step to build the entire structure of the model. This layer-by-layer method can simplify the hardware and software design of the manufacturing system [1], improve the stability of the manufacturing process, and reduce cost. Hence, FFF has become the dominant AM method in the private and semi-professional sector. However, since the overall forming depends on the mutual bonding of the pressure of the strands in the molten state, the mechanical strength is affected by the laying direction of the extruded strands, and there will be obvious anisotropic strength in different directions of the parts.

This anisotropy varies with different tool-path planning and materials. On each layer, strength is maximized when the axial directions of extruded filament strands are aligned in the load direction. The strength can drop by 40–85% when the fabricated strands are in another directions [2]. Due to temperature changes between adjacent layers, more gaps will be generated, which results in strength reduction as well. According to the literature, materials such as ABS(Acrylonitrile Butadiene Styrene) and PLA(Polylactic Acid), both as pure resin and reinforced with fibers, the strength decreased by 50-80% (ABS), 30-60% (PLA), 80-90% (reinforced ABS or PLA), respectively [3,4]. The damage locations are unpredictable when fabricating parts with a complex shape, which makes it difficult to manufacture functional components directly by FFF[5-7].

3D fabrics have interwoven fiber beams in the thickness direction, so they have better inter-laminar shear strength and fracture toughness. In this paper, the authors have utilized the path planning ideas in the 3D fabric that increases the uniformity of connections between layers through interlocked fibers. Compared to the path planning in 3D fabrics, the main challenge here is that the FFF process uses solidified polymers for manufacturing, which cannot be transferred by the mechanical mechanism such as flying shuttles. In order to realize a 3D weaving structure on a standard FFF platform, it is necessary to design new path patterns to ensure inter-layer interlocking and manufacturability. The authors propose a repetitive weaving path that can be implemented on conventional 3-axis FFF platforms and be extended to various structures as a general 3D printing infill pattern.

1.1 Related Work

1.1.1 Reducing anisotropy

Currently, there are many studies focused on reducing the anisotropic mechanical strength of FFF printed structures. Most of these works start from the perspective of the manufacturing process, improving the performance of the printed parts by optimizing the fabrication temperature, changing the geometry of the slices, and adding additional post-processing.

Collins et al.[8] used a stream of heated air to increase the interface temperature. The pre-deposition heating system was found to be useful, but the airflow disrupted the geometry of the built parts. Kishore et al.[9] demonstrated a similar pre-heating approach using infrared lamps mounted to the extruder, and the fracture energy of ABS reinforced with 20% chopped carbon fiber samples doubled when exposed to preheating. Also, the printing speed of this method is slow. Shaffer et al.[5] proposed a method to use gamma irradiating PLA samples to add cross-linking between layers without leading to excess chain scission; that method improves interlayer adhesion and reduces mechanical anisotropies. Charles et al. [10] used microwave radiation to localize heating to the weld interfaces; this approach was found to improve the fracture strength of PLA coated with carbon nanotubes by 275%, without reducing the dimensional accuracy of parts. Bhandari et al. [11] used annealing at 90°C for 240 min to strengthen the interlayer tensile strength of carbon fiber reinforced PLA specimens. These methods have high costs and are difficult to extend to standard FFF platforms.

Designing a tool-path on special surfaces is another way to reduce anisotropy. Chakraborty et al. [12] presented a tool-path generation method to deposit material in curved layers, which can be used in manufacturing thin and curved parts (shells), reducing the staircase effect as well as the number of layers and increased the strength of the parts. Singamneni et al.[13] proposed a slicing strategy that mixed curved and flat layers. The approach eliminates the staircase effect and the improved the quality of the surface and the internal structure. Duty et al.[3] provided a ‘z-pinning’ approach that deposited continuous material across multiple layers within the pre-printed through-hole structure, which can increase the tensile strength and toughness in the z-direction by more than a factor of 3.5. Etienne et al. [14] provided a volume-based method that mapping the infill path from planes to curved surfaces. This method can be printed on a standard 3-axis FFF printer and reduces the internal porosity and

fragilities. Chengkai et al.[15] proposed a method to reduce supporting structures as much as possible by printing different model areas along with different directions. The key of this algorithm is to minimize areas with large overhangs. They also proposed a new system of 5 degrees of freedom (DOF) 3D printing which is employed by robotic arms [16]; that method can manufacture solid models by few supporting structures, and the print process is collision-free. Guoxin et al.[1] proposed a method to lay the tool-path along the direction of the stress field of a solid model in a multi-axis printing system. This method can reinforce mechanical strength, and the whole printing process is guaranteed to be collision free. Most methods rely on multi-axis equipment and can only be applied to specific structures. Therefore, it is difficult to improve the isotropy of mechanical strength.

1.1.2 Weaving in AM

Knitted fabrics are widely used in clothing because of their parallel and interlaced properties, which are formed by weaving. In comparison to knitted fabrics, which are made of a single layer, 3D weaving owns more than one layer. The advantage of 3D weaving parts is the delamination resistance in the finished part provided by fibers aligned in the Z-direction[17]. Some applied research efforts have focused on the use of AM to demonstrate the shape of weaving structures. Haruki et al.[18] proposed a method to fabricate soft and flexible textiles by an FFF 3D printer. The authors used a movement control of the printer head to alternately weave the soft fibers across a row of pillars. Quan et al.[19-21] proposed a method of multidirectional manufacturing interlock woven structures, which uses ABS as the feedstock of model material, while water-soluble filament served as support material. They also tested the effect of yarn diameter and knitting angle on the mechanical properties. Beecroft [22] et al. proposed a method to print a weft knitted structure by using an SLS 3D printer with polyamide (PA) powder, and the samples showed stretch and extensibility. Panetta et al.[23] proposed a method to create deformable objects via copy and paste specific microstructures. Their approach could manufacture controlled-anisotropy samples.

Dickson et al.[24] proposed a method to use continuous carbon fiber filament via G-code to generate a few layers with woven-hole structures. This sample has better mechanical properties than the sample with direct punching holes. Partsch et al.[25] used a 3D CAD design software to design three different plain weave samples, and converted them to the triangle mesh models. Then they manufactured the entity by an FFF 3D printer with ABS, and subsequently compared the shear deformation of the three samples. Haruki et al.[26] proposed a method by increasing and decreasing the amount of material extruded during printing process to generate a single layer object, which looks like a woven structure. Zhang [27] used shape memory polymer and PLA to print circular braided tube preforms and analyzed the effect of braiding angle, tube wall thickness and temperature. Li et al.[28] designed a PLA-based composite. The printed PLA braiding structures were integrated with two types of resins. A compression test indicated the variety of the mechanical properties for the usage of different resins. Most similar methods are only suitable for generating simple weaving structures. Printing of fused filaments with 3D fabric morphology for different geometric structures is still a challenging task.

2. Weaving Infill Pattern

2.1 Inter-laminar interwoven

Different from looms, FFF equipment uses thermoplastic, elastomeric or thermosetting materials; these material cannot move after curing, and the print nozzle cannot move between two layers like a shuttle. Firstly, one has to regard the fused filament extruded from the printer nozzle as yarn. Then m parallel fused filaments are combined as a yarn strip for weaving. As shown in **Fig. 1(a),** if the used nozzle diameter is w, and the distance between two parallel deposit fibers is 0, the width of every yarn strip is $w \times m$. To fabricate the weaving structure, the nozzle of the 3D printer needs to move up and down in the z-direction.

The moving trajectory of the nozzle in the x-z plane is indicated by the green line in **Fig. 1(b)**. We define the fibers spread along the x-direction as warp yarns, and the fibers perpendicular to it as weft yarns. The warp covers and embeds the lower weft along the green arrow so that the two layers can form an interlaced relationship. **Fig.1(c)** shows a two-layer physical model printed using the FFF platform. The position where the two layers are interlaced is marked by red lines. The setting layer height is h, the deposition spacing is h. So, the thickness of the yarn is h. This way can be used in most three-axis FFF platforms on the market.

2.2 Overall strategy of 3D weaving infill pattern

Due to the interwoven characteristics of yarns in the 3D weaving structure, the heights of each layer are different. To realize the interwoven structure between every two layers on the FFF platform, the authors have designed a 3D weaving mode generation strategy. This strategy consists of a repetitive structure that continuously cycles in the direction of thickness to form a scalable 3D structure.

Fig. 2(a) shows a 3D weaving structure printed with repetitive pattern. Firstly, an initial layer is printed. Then, some repetitive layer groups are printed in a loop until the specified height is reached. As shown in **Fig. 2(b)**, the initial layer l_s is displayed in red, and the green ones are layer groups l_j (j=1,2,3,4…n). Each layer group l_j contains 5 sublayers represented by $l_{(j,k)}$, where k (k=1,2,3,4,5) represents the k-th sublayer in the repetitive structure l_j.

This strategy generates a 3D orthogonal woven fabric. In each repetitive layer group l_j, the lower sublayer $l_{(j,k)}$ and upper sublayer $l_{(j,k+1)}$ are interwoven. Every two repetitive structures are also interwoven because the sublayer $l_{(j,5)}$ and sublayer $l_{(j+1,1)}$ are interlaced. Therefore, this strategy guarantees unlimited extension in the direction of thickness. One can use the 3D orthogonal woven fabric as an infill pattern to fill a 3D space defined by any input models.

2.3 Path planning

The initial layer l_s is the first layer of the 3D weaving infill pattern, which is printed on the bottom shell. The tool-path layout of l_s shown in **Fig. 3 (a)**. Each weft yarn strip consists of m yarns. The distance between two neighbor strips is $w \times m$. The layer height is h. After the initial layer is printed, the weft yarn layer covers half the area of the current processing plane. The current height map of this layer is shown in **Fig.3 (b)**, where the cyan area represents height h, and the white areas height 0. The black strips parts on the left (warp direction) and the bottom (weft direction) of **Fig.3 (b)** give the corresponding orthogonal views.

The authors used the same configuration as the initial layer l_s in the repetitive layer group l_j including the strip width, layer height and distance between two neighbor strips. The tool-path layout on $l_{(j,1)}$ is shown in **Fig. 4(a)**. After $l_{(j,1)}$ is printed, the height map of $l_{(j,1)}$ is shown in **Fig. 4(c)**. There are three types of heights on the current layer. In order to clearly demonstrate the change of the height map before and after printing, the authors repeatedly give the height map of the last layer on the left side of the **Fig. 4**.

Fig. 5(a) shows the tool-path layout on $l_{(j,2)}$. As shown in **Fig. 5(c)**. There are two types of heights on the current layer after $l_{(j,2)}$ is printed. Although three layers have been printed, the highest layer height is still $2h$ because the new material is not deposited at the highest point. In the warp and weft projections, the original interwoven parts of the upper and lower layers are occluded, showing a new printed part.

$l_{(j,3)}$ is a special layer in the repetitive layer group. As shown in **Fig. 6 (a)**, the z-axis in $l_{(j,3)}$ does not need to change because the height on x-direction is constant. The height map shown in **Fig. 6 (c)** demonstrates the impossibility to interweave the fibers between layer $l_{(j,3)}$ and the next layer $l_{(j,4)}$. Therefore, the doubled amount of extruded material resulted in the doubled layer height as well. Then the weft yarn on the next layer $l_{(j,4)}$ can be embedded into the area between two warp yarn strips.

$l_{(j,4)}$ is the fourth sublayer of the repetitive layer group and the tool-path on it is shown in **Fig. 7(a)**. There are three types of heights on the height map shown in **Fig. 7(c)**. after printing the weft yarn strips.

The tool-path layout on the final sublayer $l_{(j,5)}$ is shown in **Fig. 8(a)**. After the warp yarn strips are printed on $l_{(j,5)}$, the height map of the current layer is shown in **Fig. 8(c)**. The orthogonal views in **Fig. 8(c)** demonstrates how the warp and the weft yarn strips are interwoven and embedded to each other.

Once $l_{(j,5)}$ is printed, the height map on the current layer is the same as l_s. **Fig. 9** compares the height map on the initial layer l_s and the fifth sublayer $l_{(j,5)}$. The patterns are identical, so the print of the layer group can be repeated until the specified height is achieved. The total heights of c cycles layer groups are $3 \times c \times h$ *and* $3 \times c \times h + h$.

3. 3d Weaving Printing

3.1 General process

A standard FFF printed part consists of outer shells, bottom layers, top layers, and infills. The first three parts ensure the surface quality. The infills provide changeable internal structures that can regulate weight, porosity, distribution of stress, etc. **Fig. 10** shows a processing flow that integrated the 3D weaving infill pattern to generate G-code for the 3-axis FFF platform. The input model defines the processing area and print parameters. The parameters contain the FFF printing configuration and the control parameters for the 3D weaving infill pattern. After the printing direction is determined, a standard model slicing process obtains information on each layer.

Compared to other infill patterns used in 3D printing, the 3D weaving infill pattern has different layer heights. To avoid interference, the printing order of shells and infills is scheduled based on the layer height. Finally, the corresponding G-code is generated according to different printing platforms.

3.2 Infill density

One of the advantages of the FFF technology is that it can select the appropriate infill density for different models, which makes the printing process spend less time with less material consumption while obtaining enough mechanical strength. In the actual printing process, we output all number of m lines, and extrusion rate e (the ratio of material extruded by nozzle to distance passed, e is related to h) is standard used (standard $e=h/6$), then the infill density is 100 %. If the number of d lines ($1<=d<m$) are outputs, and the extrusion rate is $r\times e$, the infill density is $r\times d/m$. Since d and m are integers, when we use standard e, the infill density is discrete. If the infill density of the model is set, an appropriate m, r and d can be selected to make the actual filling rate closest to the predefined infill density. As shown in **Fig. 11**, all cubic lengths, widths, and heights are 40mm × 40mm × 1.8mm, w=0.4mm, h=0.15mm, r=1. Due to the increase of the filling rate, the cube is filled with more areas. Once the filling rate is set, although using different m, the final amount of extrusion material is the same.

Fig. 12 shows the 3D weaving infill patterns with different parameters. As displayed in **Fig. 12(a)**, parameter m can be used to control the size of the void. However, the weaving path moves frequently in the z-axis direction and eventually leads to over-concentration and crevices in the deposited material. Increasing material extrusion improves print quality, but also affects the actual fill density. In our test, the filling effect would be much better if increasing the extrusion rate by 70%.

3.3 Algorithm for 3D weaving printing

We use **Algorithm 1**. to print both the 3D woven infill patterns and shells together. This algorithm is divided into **Algorithm 1.1** and **Algorithm 1.2**. The first one slices the inputted model and generates the tool-path, which calls **Algorithm 1.2** to get printing order of the outer contours and the sublayers of infills.

In order to express the whole process more clearly, the algorithm for 3D weave printing is given in the form of a flowchart shown in **Algorithm 1.1**. Assuming the printing direction, input 3D model S, infill density u, nozzle diameter w, shell thickness t_1, base thickness t_2, 3D weaving control parameters h, m are given. First set the layer height of the slice is h, and the contour information of each layer $\Omega_1[1...n_1]$ is

obtained. Then, the number of base slices n_2 is obtained according to t_2, and the contour data except the base are taken out from Ω_1. The contour of the initial layer is determined according to $\Omega_1[n_2+1]$.

As shown in **Fig. 13(a)**, different color squares represent different repetitive layer groups, each layer group relatively increases the height of $3\times h$. Due to the uneven initial layer, each repetitive layer group actually across the height of $4\times h$, so each repetitive layer requires 4 specific adjacent sublayers as the contour. The top sublayer of a repetitive layer group shares an outer contour with the bottom sublayer of the next repetitive layer group. Then every four specific sublayers in $\Omega_1[n_2+1\ldots n_1]$ are used as a repetitive layer group and all repetitive layer groups contour information $\Omega_2[j_1\ldots j_n]$ are obtained.

Algorithm 1. 3D Weaving Pattern Fill Different Structure

For each repetitive layer, the bounding box $B[j_1\ldots j_n]$ is obtained and filled with the bounding box by 3D weaving, and the point set $X[j_1\ldots j_n]$ is obtained. Finally, we can get the points of true output to G-code according to u.

As shown in **Algorithm 1.2**, each repetitive layer needs to print the outer contour according to t_1, Ω_1, and X. Printing outer contour is divided into two parts, the first part is to ensure that the internal 3D weaving filling and the outer contour are bordering; the second part is that every sublayer should judge the points inside the out contour.

For the first part, the 3D weaving filling mode is divided into five sublayers, where each sublayer crosses the height of $2\times h$. Since the height of the outer contour is h, the contour printing order strategy like **Algorithm 1.2** is used to ensure that the 3D weaving filling in each sublayer will be bordered with the outer contour.

For the second part, as shown in **Fig. 13(a)**, due to the different Ω_2 may share the same Ω_1, the specific layer heights of Ω_1 are marked in the diamond box. So, each **judge** function input includes the corresponding layer height of Ω_1 and X. Finally, determines whether the odd and even times of intersection in Ω_1 by scanning the points in X one by one. **Fig. 13(b)-(f)** shows the input model as a regular hexagonal column, filled with 3D weaving modes by different density and m.

4. Experiments

To test the mechanical properties of 3D printing parts with 3D weaving infills, two groups of experiments were designed. The used filament is PLA, the 3D printer is a standard 3-axis FFF printer with a Marin motherboard. The three points bending mechanical properties and tensile properties were analyzed on a WDW-1 material testing machine (WDW-1, SONGDUN Corp. China).

4.1 Bending test

The loading mode of test samples is shown in **Fig. 14(a)**, span is 48mm. The 3 points bending test includes four groups of samples. The used test standard is ISO 14125:1998. As shown in **Fig. 14(b)(c)**, the four group samples are fabricated with tool-paths of zig-0, zig-90, weaving-0, weaving-90, respectively. The zig-0 and zig-90 patterns are printed with the zigzag path, and the number means the angle of filaments and the load direction. The weaving-0 and weaving-90 are printed with our 3D weaving path, the number specifies the direction of the initial layer.

Table 1. Experiment data of three points bending

Fill Pattern	Layer Thickness (mm)	Median of Max Force(N)	Average of Max Force(N)	Absolute Deviation	Average Weight(g)
zig-0	3.2	255.674	255.705	18.751	116.146
zig-90	3.15 and 3.3	171.0283	175.7113	7.142	116.0607
weaving-0	3.15 and 3.3	201.1275	197.9608	11.875	116.3568
weaving-90	3.15 and 3.3	217.3216	218.1693	10.485	116.581

Each group consists of five samples. The length, width, and height of zig filling samples are 98mm × 24mm × 3.2mm. The heights of weaving filling samples are 3.15mm, and 3.3mm, due to the fact that the 3D weaving fill structure is uneven for every sublayer. The parameters of weaving are: h=0.15mm, u=1.0, w=0.4mm, m=14.

Three points bending test data histogram and specific data, as well as physical samples, are shown in **Table.1, Fig. 14(c)**, and **Fig. 15**.

4.2 Tensile test

To further investigate the relationship between the mechanical properties of 3D weaving and the parameter m, the length and width of the first group experiments were extended to the second group of experiment samples. The thickness of the sample was 1 mm (the 3D weaving thickness was 0.9 mm and 1.05 mm). Twelve different paths were used to test the tensile properties. Among them, ten 3D weaving paths were used, and five samples were printed for each path, which are zig-0, zig-90, weaving-0(m=2), weaving-90(m=2), weaving-0(m=4), weaving-90(m=4), weaving-0(m=6), weaving-90(m=6), weaving-0(m=10), weaving-90(m=10), weaving-0(m=14), weaving-90(m=14).

The physical samples and specific data, loading mode of samples, as well as data histogram, are shown in **Fig. 16, Table.2,** and **Fig. 17(a).**

4.3 Discussion

The evaluation of the bending test showed that the zig-90 samples had the best mechanical strength, and the zig-0 had the worst strength. The difference between the two groups was 45.71%. The zig-0 group had good tenacity and all five samples did not break at maximum load. All the samples in the zig-90 group were broken. The bending strength of the two group samples with the 3D weaving path is located

between zig-90 and zig-0, and the mechanical difference between them is 10.21%, of which the maximum bending strength of the better weaving-90 reaches 85.54% of zig-90. Since the zig-0 is filled along the direction of bending force, the three-point bending mechanical properties of zig-0 are much better than those of zig-90. The main reason for the difference between two weaving-90 and weaving-0 is that the third sublayer of weaving-90 is the same as a zigzag filling along the stress direction and the material extrusion amount is twice that of the other layers, while weaving-0 is perpendicular to the stress direction.

Table 2. Experiment data of double points pulling

infill Pattern	Layer Thickness(mm)	Median of Max Force(N)	Average Max Force(N)	Absolute Deviation
zig-0	1	438.2489	458.8456	21.268
zig-90	1	149.9091	149.06	6.496
weaving-0(m=2)	0.9 and 1.05	380.526	398.431	17.6315
weaving-90(m=2)	0.9 and 1.05	383.5665	399.328	14.873
weaving-0(m=4)	0.9 and 1.05	366.488	376.242	28.0072
weaving-90(m=4)	0.9 and 1.05	378.089	379.9516	20.24272
weaving-0(m=6)	0.9 and 1.05	381.722	382.9742	10.02664
weaving-90(m=6)	0.9 and 1.05	374.392	376.553	14.56
weaving-0(m=10)	0.9 and 1.05	388.087	390.9712	16.1034
weaving-90(m=10)	0.9 and 1.05	425.774	417.2544	15.71896
weaving-0(m=14)	0.9 and 1.05	335.4657	328.61292	12.484
weaving-90(m=14)	0.9 and 1.05	367.7812	360.95028	24.256

In the tensile test, the tensile properties of the group with 3D weaving paths are also between two groups of samples with zigzag paths. The zig-0 group has the best tensile strength, which shows that the direction of the filaments aligning has a significant effect on the mechanical properties. The tensile properties of weaving-90(m=10) can reach 91.05% of zig-0. The properties of weaving-90(m=10) are slightly better than weaving-0(m=10). More importantly, with the decrease of m value, the anisotropy of the samples with 3D weaving structures decreases gradually and tends to 0, which is far less than that of zig filling.

The 3D weaving infill pattern can be utilized if the designed FFF products requires low anisotropic strength properties. However, the 3D weaving path does not further improve the mechanical performance of the samples as we thought. The main reason is that the frequent movement of the nozzle leads to more microscopic cracks.

In the actual printing process, the smaller of m, the greater the probability of material accumulation or pores in the 3D weaving structure. As shown in **Fig.17(b)**, during the frequently downward movement of the nozzle, the fused filaments will be compressed and the area of the compressed area will be slightly larger, which leads to the following layer generate voids; In the process of upward movement of the nozzle, the fused filaments will drop slightly due to inertia, which may lead to the accumulation of materials in the process of rising, which requires appropriate adjustments to the printer speed and extrusion rate.

Decreasing m by 1 will increase the printing time by 10%. There are two main reasons: first, the smaller the *m* value, the more times the z-axis moves, resulting in an increase in printing time; second, 3D weaving structure only prints half of the plane in each sublayer, and it takes time for the nozzle to move to the next plane for printing.

5. Conclusion

The problem of the anisotropic strength due to the direction of filaments deposition is unavoidable in FFF process. In this paper, a 3D weaving path planning method is introduced to reduce the anisotropy of printed parts. The method can be implemented on the standard FFF platforms and generate structures with interlocking and embedding layers.

A five-layer repetitive structure was designed, which enables the weaving path to be infinitely extended in the thickness direction, resulting in an infill pattern similar to the 3D orthogonal woven fabric. The strategy can be used in the manufacture of different geometric models by further synchronizing the printing of shells and infills. The experimental results show that the weaving path can make the print showing approximate aesthetic properties in all directions.

The main limitation of this work is the existance of an embedded layer in the five layers of the repetitive layer groups rather than totally interweaving each other, it affects the connection strength between layers. In addition, the heights of shell and infills are not consistent. The frequent moving up and down in print heads can also have potentially negative effects on the surface quality and strength of the actual printed part. This work presents a 3D weaving infill pattern which can be improved in future work and become a stable and universal infill pattern for FFF platform.

Declarations

Funding: Natural 3D: Bio-based fibre/particle reinforced thermoplastics efficiently used by additive manufacturing in the load path direction (860384, FFG Austria)

Conflicts of interests: The authors have no conflicts of interest to declare that are relevant to the content of this article.

Data: The authors declare that the experimental data are true and valid.

Code availability: The code is not currently public.

Authors' contribution statements: Yuan Yao presented the conception and drafted the framework of the article. Cheng Ding designed the algorithms, tested experiments, and the drafted article. Lanlan He revised the article. Mohamed Aburaia and Maximilian Lackner made the critical revision of the paper.

References

1. Fang G, Zhang T, Zhong S, Chen X, Zhong Z, Wang CCL (2020) Reinforced FDM. ACM Transactions on Graphics 39 (6):1-15. doi:10.1145/3414685.3417834

2. Bellini A, Journal SGJRP (2003) Mechanical characterization of parts fabricated using fused deposition modeling. 9 (4):252-264. doi:10.1108/13552540310489631

3. Duty C, Failla J, Kim S, Smith T, Lindahl J, Kunc V (2019) Z-Pinning approach for 3D printing mechanically isotropic materials. Additive Manufacturing 27:175-184. doi:10.1016/j.addma.2019.03.007

4. Turner BN, Strong R, Gold SAJRPJ (2014) A review of melt extrusion additive manufacturing processes: I. Process design and modeling. 20 (3):192-204. doi:/10.1108/RPJ-01-2013-0012

5. Shaffer S, Yang K, Vargas J, Di Prima MA, Voit WJP (2014) On reducing anisotropy in 3D printed polymers via ionizing radiation. 55 (23):5969-5979. doi:10.1016/j.polymer.2014.07.054

6. Rankouhi B, Javadpour S, Delfanian F, Letcher TJJoFA, Prevention (2016) Failure Analysis and Mechanical Characterization of 3D Printed ABS With Respect to Layer Thickness and Orientation. doi:10.1007/s11668-016-0113-2

7. Letcher T, Rankouhi B, Javadpour S Experimental Study of Mechanical Properties of Additively Manufactured ABS Plastic as a Function of Layer Parameters. In: Asme Imece, 2015. doi:10.1115/IMECE2015-52634

8. Chairperson CDSC (1985) Fused deposition modeling with localized pre-deposition heating using forced air. Springer-Verlag,

9. Kishore V, Ajinjeru C, Nycz A, Post B, Lindahl J, Kunc V, Duty CJAM (2016) Infrared preheating to improve interlayer strength of big area additive manufacturing (BAAM) components. 14:7-12. doi:10.1016/j.addma.2016.11.008

10. Charles, Sweeney, Blake, Lackey, Martin, Pospisil, Advances TJS (2017) Welding of 3D-printed carbon nanotube-polymer composites by locally induced microwave heating. doi:10.1126/sciadv.1700262

11. Bhandari S, Lopez-Anido RA, Gardner DJ (2019) Enhancing the interlayer tensile strength of 3D printed short carbon fiber reinforced PETG and PLA composites via annealing. Additive Manufacturing 30. doi:10.1016/j.addma.2019.100922

12. Chakraborty D, Aneesh Reddy B, Roy Choudhury A (2008) Extruder path generation for Curved Layer Fused Deposition Modeling. Computer-Aided Design 40 (2):235-243. doi:10.1016/j.cad.2007.10.014

13. Singamneni S, Joe RA, Huang B (2012) Adaptive Slicing for Fused Deposition Modeling and Practical Implementation Schemes. Advanced Materials Research 428:137-140. doi:10.4028/www.scientific.net/AMR.428.137

14. Etienne J, Ray N, Panozzo D, Hornus S, Lefebvre SJAToG (2019) CurviSlicer: Slightly curved slicing for 3-axis printers. 38 (4). doi:10.1145/3306346.3323022

15. Wu C, Dai C, Fang G, Liu Y-J, Wang CCL (2020) General Support-Effective Decomposition for Multi-Directional 3-D Printing. IEEE Transactions on Automation Science and Engineering 17 (2):599-610. doi:10.1109/tase.2019.2938219

16. Dai C, Wang CCL, Wu C, Lefebvre S, Fang G, Liu Y-J (2018) Support-free volume printing by multi-axis motion. ACM Transactions on Graphics 37 (4):1-14. doi:10.1145/3197517.3201342

17. Wu R, Harvey C, Zhang JX, Kroszner S, Hagan B, Marschner S (2020) Automatic structure synthesis for 3D woven relief. ACM Transactions on Graphics 39 (4). doi:10.1145/3386569.3392449

18. Takahashi H, Kim J 3D Printed Fabric: Techniques for Design and 3D Weaving Programmable Textiles. In: the 32nd Annual ACM Symposium, 2019.

19. Quan Z, Larimore Z, Qin X, Yu J, Mirotznik M, Byun J-H, Oh Y, Chou T-W (2016) Microstructural characterization of additively manufactured multi-directional preforms and composites via X-ray micro-computed tomography. Composites Science and Technology 131:48-60. doi:10.1016/j.compscitech.2016.05.015

20. Quan Z, Suhr J, Yu J, Qin X, Cotton C, Mirotznik M, Chou T-W (2018) Printing direction dependence of mechanical behavior of additively manufactured 3D preforms and composites. Composite Structures 184:917-923. doi:10.1016/j.compstruct.2017.10.055

21. Quan Z, Wu A, Keefe M, Qin X, Yu J, Suhr J, Byun J-H, Kim B-S, Chou T-W (2015) Additive manufacturing of multi-directional preforms for composites: opportunities and challenges. Materials Today 18 (9):503-512. doi:10.1016/j.mattod.2015.05.001

22. Beecroft M (2019) Digital interlooping: 3D printing of weft-knitted textile-based tubular structures using selective laser sintering of nylon powder. International Journal of Fashion Design, Technology and Education 12 (2):218-224. doi:10.1080/17543266.2019.1573269

23. Panetta J, Zhou Q, Malomo L, Pietroni N, Cignoni P, Zorin D (2015) Elastic textures for additive fabrication. ACM Transactions on Graphics 34 (4):1-12. doi:10.1145/2766937

24. Dickson AN, Ross K-A, Dowling DP (2018) Additive manufacturing of woven carbon fibre polymer composites. Composite Structures 206:637-643. doi:10.1016/j.compstruct.2018.08.091

25. Partsch LN, Vassiliadis S, Papageorgas P 3D PRINTED TEXTILE FABRICS STRUCTURES. In: 5th International Istanbul Textile Congress 2015: Innovative Technologies "Inspire to Innovate", 2015.

26. Takahashi H, Miyashita H (2016) Thickness Control Technique for Printing Tactile Sheets with Fused Deposition Modeling. Paper presented at the Proceedings of the 29th Annual Symposium on User

Interface Software and Technology - UIST '16 Adjunct, doi: 10.1145/2984751.2985701

27. Zhang W, Zhang F, Lan X, Leng J, Wu AS, Bryson TM, Cotton C, Gu B, Sun B, Chou T-W (2018) Shape memory behavior and recovery force of 4D printed textile functional composites. Composites Science and Technology 160:224-230. doi:10.1016/j.compscitech.2018.03.037

28. Li Z, Chen G, Lyu H, Ko F (2018) Experimental Investigation of Compression Properties of Composites with Printed Braiding Structure. Materials (Basel) 11 (9). doi:10.3390/ma11091767

Figures

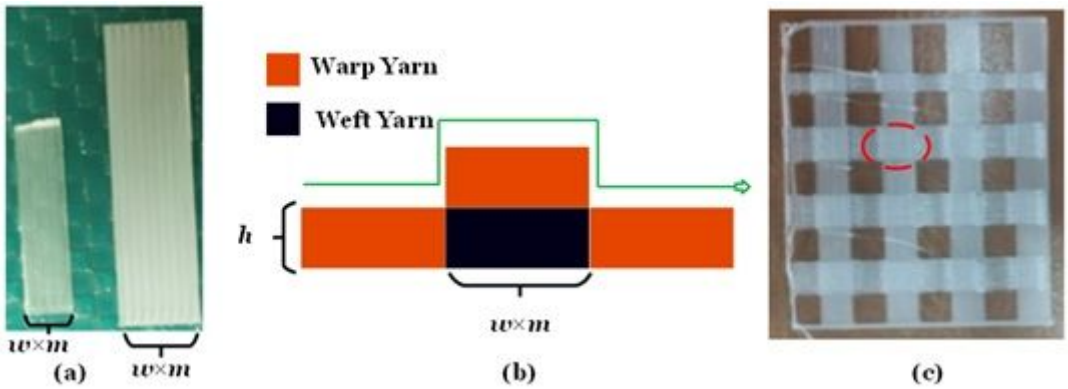

Figure 1

FFF weaving scheme. (a) Two yarn strips. (b) Warp and weft yarn strips. (c) Two-layers printed model

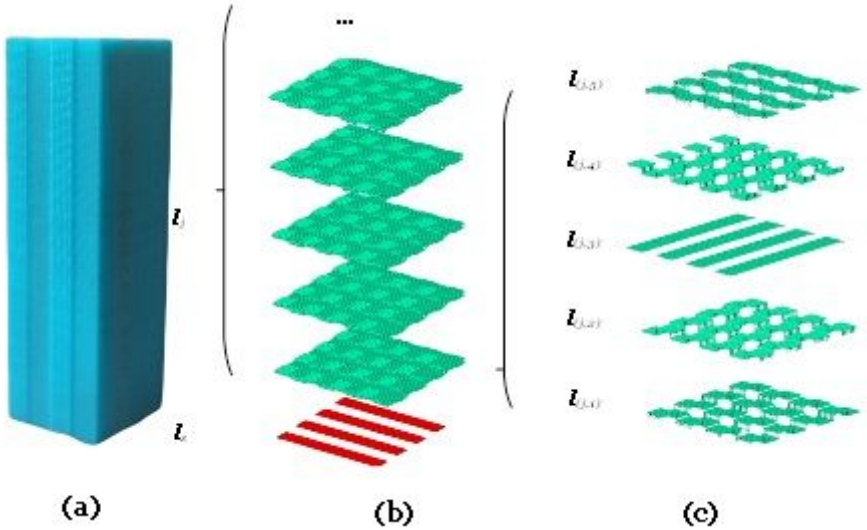

Figure 2

3D weaving structure. (a) FFF printed 3D weaving model. (b) Red: initial layer, Green: repetitive layers. (c) One repetitive layer is constituted by five sublayers

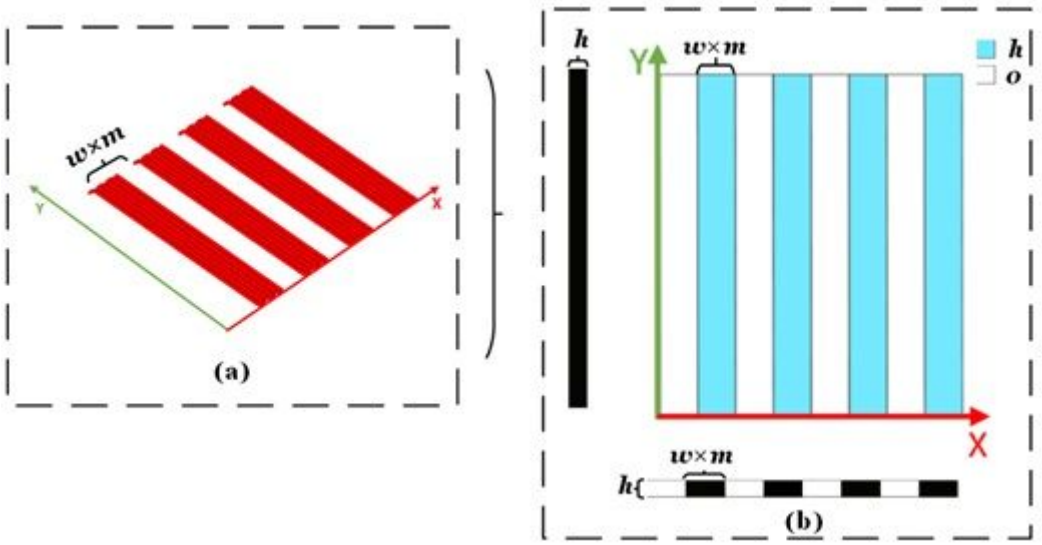

Figure 3

Tool-path on ls. (a) Initial layer ls. (b) Height map ls

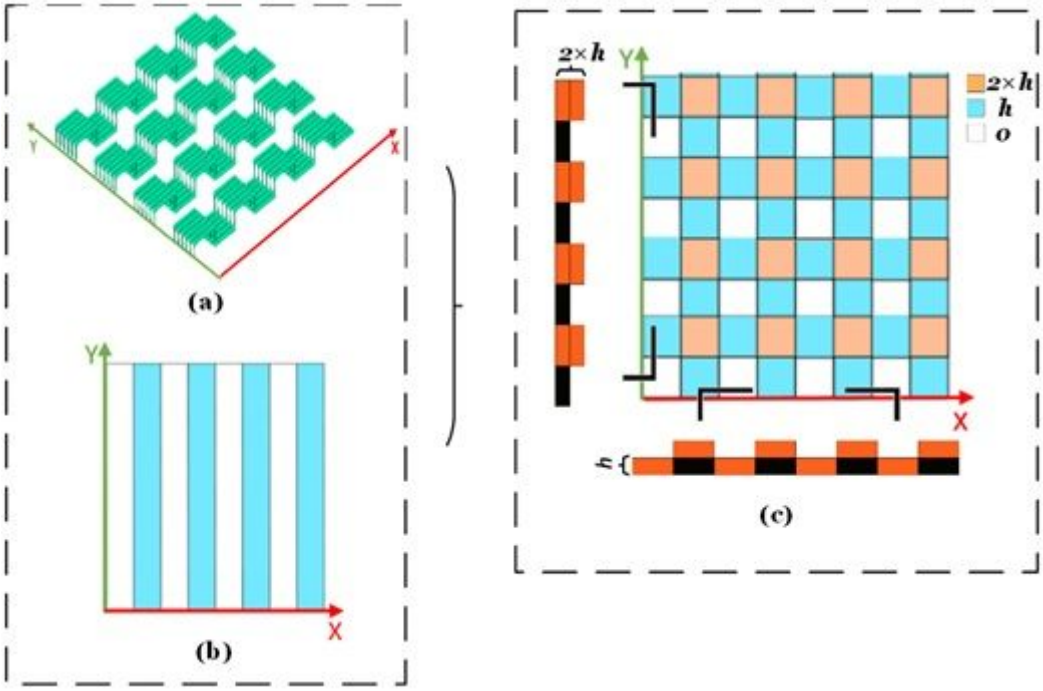

Figure 4

Tool-path on l(j,1). (a) Sublayer l(j,1). (b)Height map on ls. (c) Height map on l(j,1)

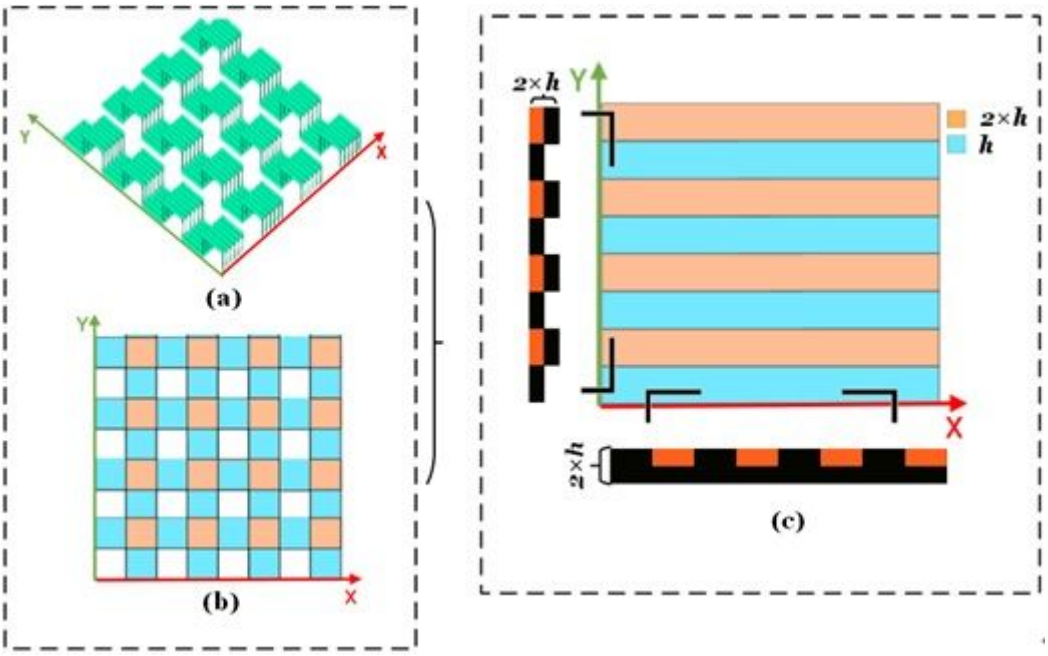

Figure 5

Tool-path for l(j,2). (a) Sublayer l(j,2). (b)Height map on l(j,1). (c) Height map on l(j,2)

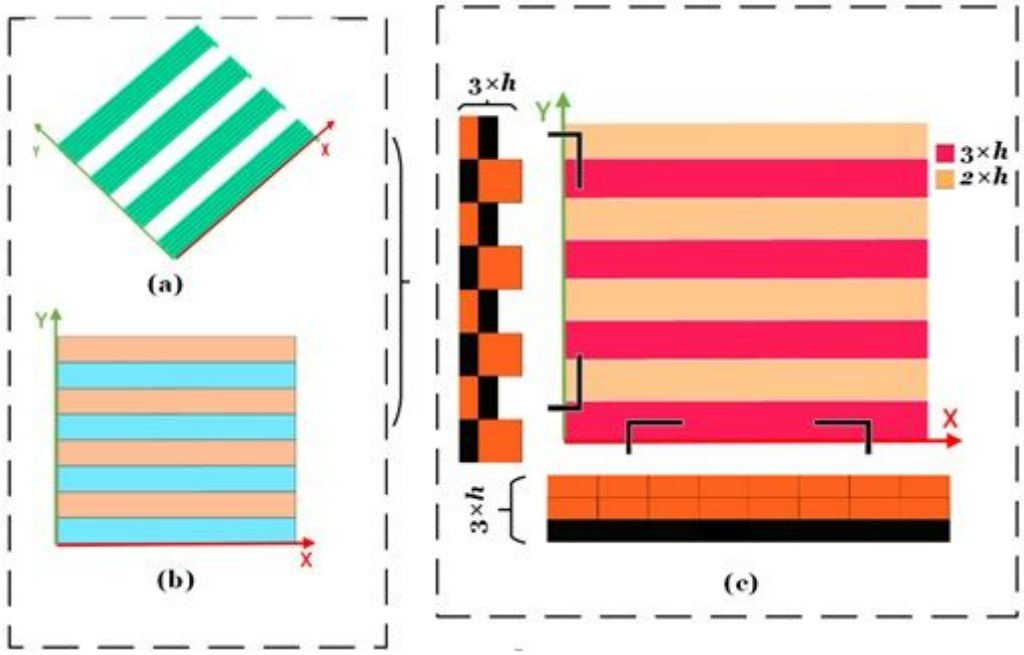

Figure 6

Tool-path for l(j,3). (a) Sublayer l(j,3). (b)Height map on l(j,2). (c) Height map on l(j,3)

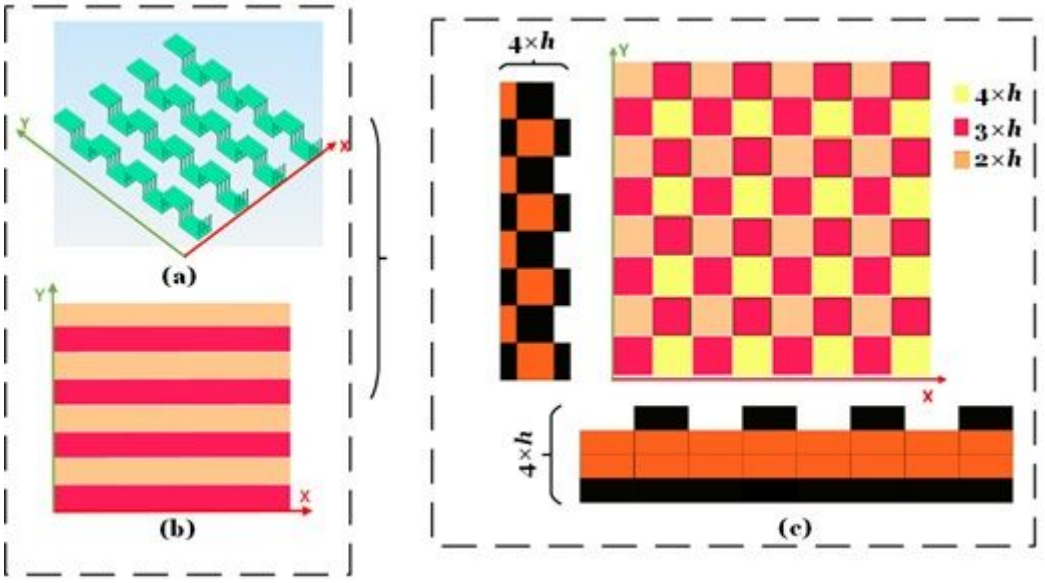

Figure 7

Tool-path for l(j,4). (a) Sublayer l(j,4). (b)Height map on l(j,3). (c) Height map on l(j,4)

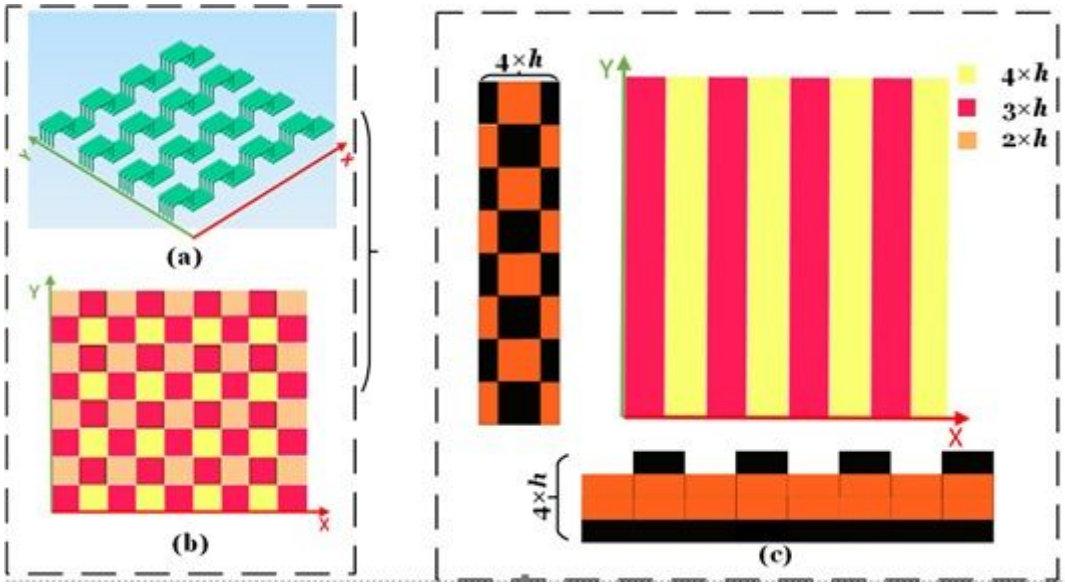

Figure 8

Tool-path for l(j,5). (a) Sublayer l(j,5). (b)Height map on l(j,4). (c) Height map on l(j,5)

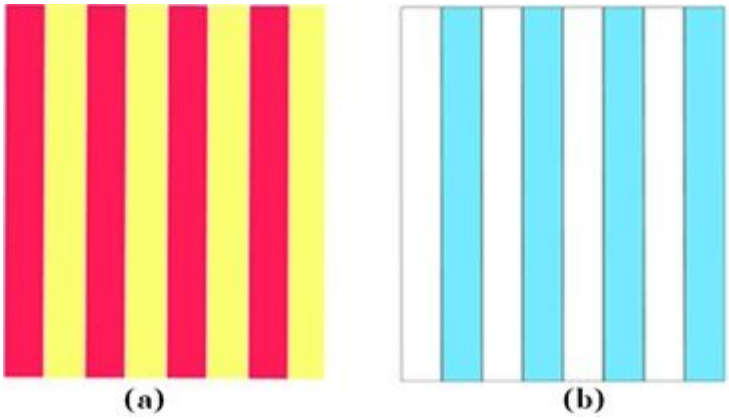

Figure 9

Comparison of height maps. (a) Height map on I(j,5). (b) Height map on Is

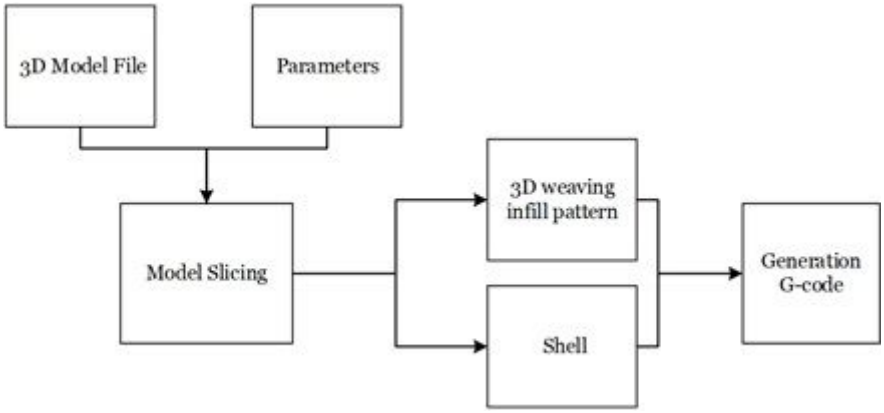

Figure 10

Flow diagram of 3D weaving print

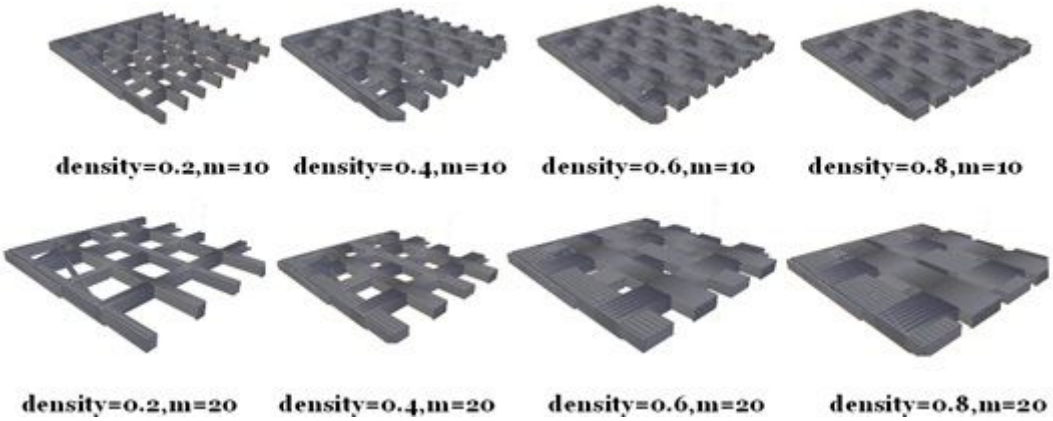

Figure 11

Infill density and pattern control

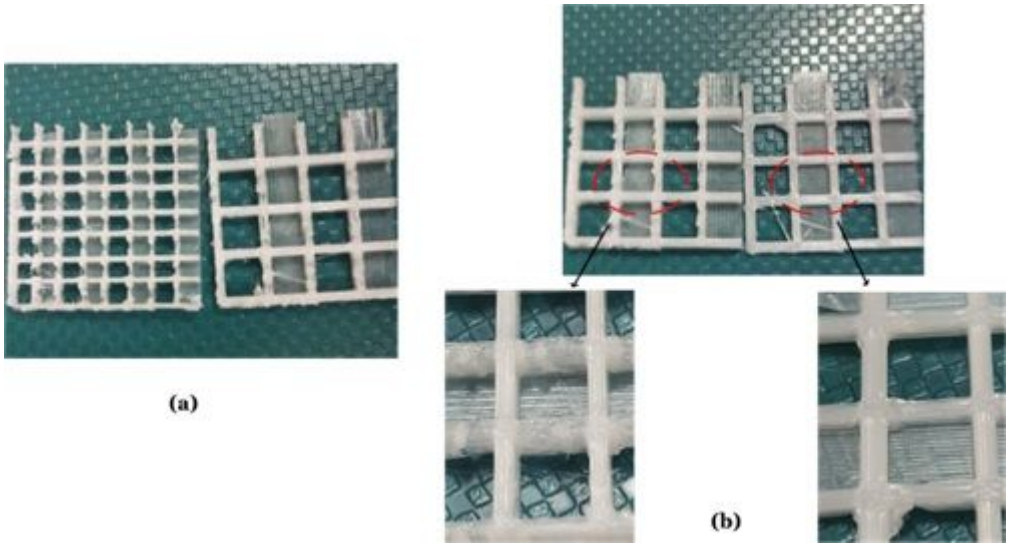

Figure 12

Printed infill patterns with different density, r and m. (a) Density=0.2, m=5, r=1 (left) and density=0.2, m=10, r=1 (right). (b) Density=0.2, m=5, r=1 (left) and density=0.34, m=5, r=1.7 (right)

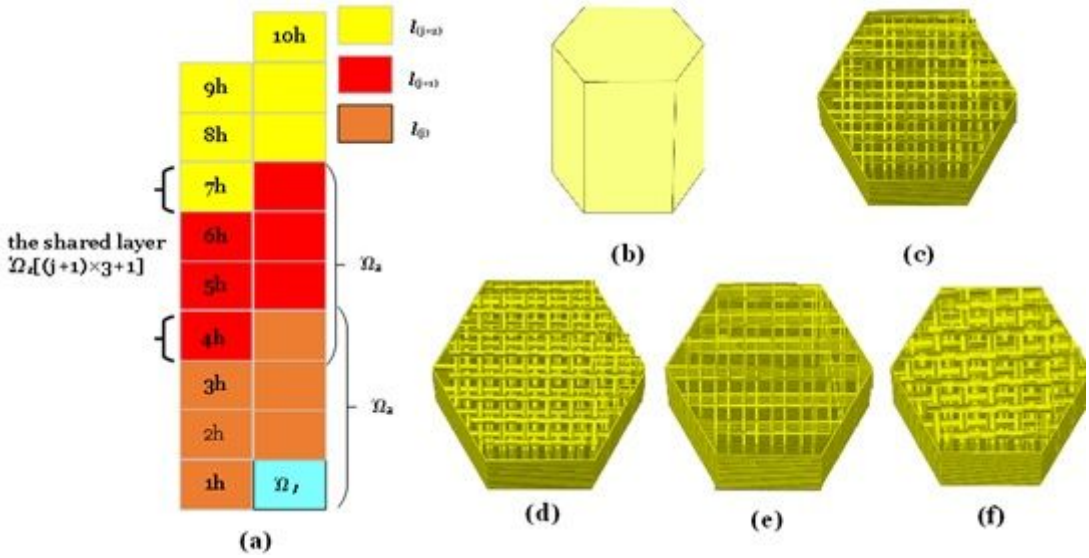

Figure 13

Examples of 3D weaving printing (a) Up four contours and low four contours share a common contour. (b) Side view of model. (c) Density=0.33, m=6. (d) Density=0.66, m=6. (e) Density=0.25, m=8. (f) Density=0.75, m=8

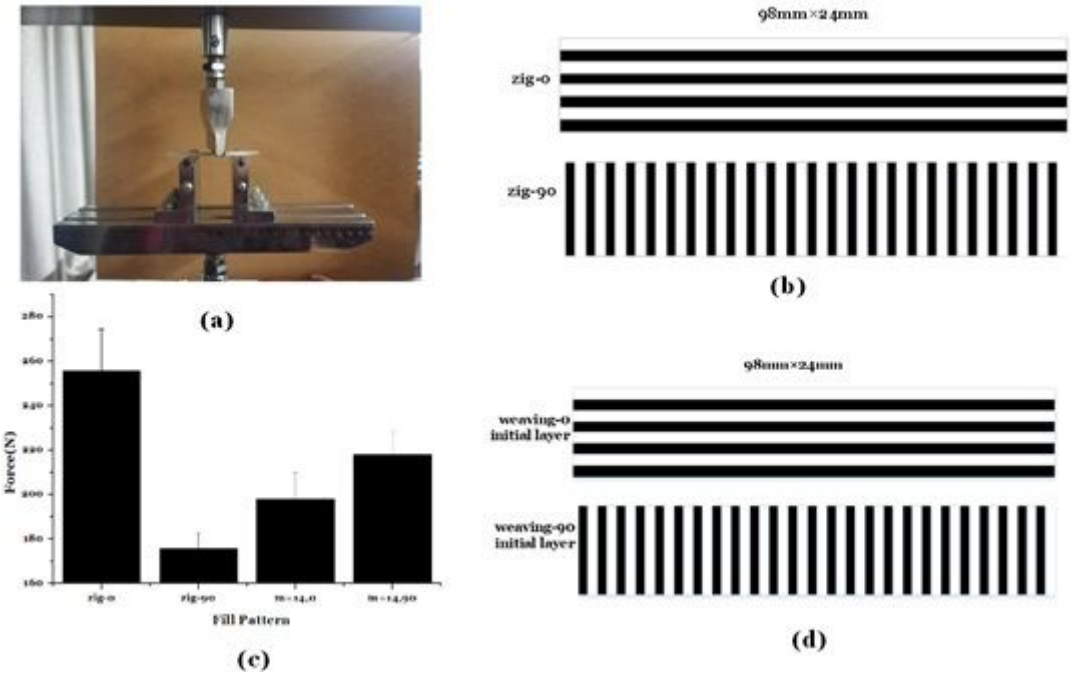

Figure 14

a) Three points bending. (b) Two zig paths which print direction are orthorhombic. (c) Two weaving path's initial layers which print direction are orthorhombic. (d) Column chart: X-axis is filling pattern, Y-axis is the average of max force

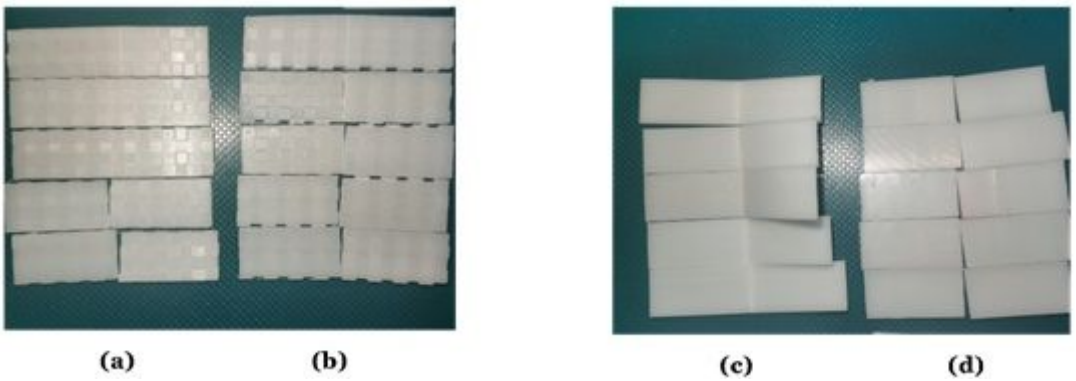

Figure 15

Printed samples with Zigzag and 3D weaving. Material: PLA. (a) weaving-90, (b) weaving-0, (c) zig-0, (d) zig-90

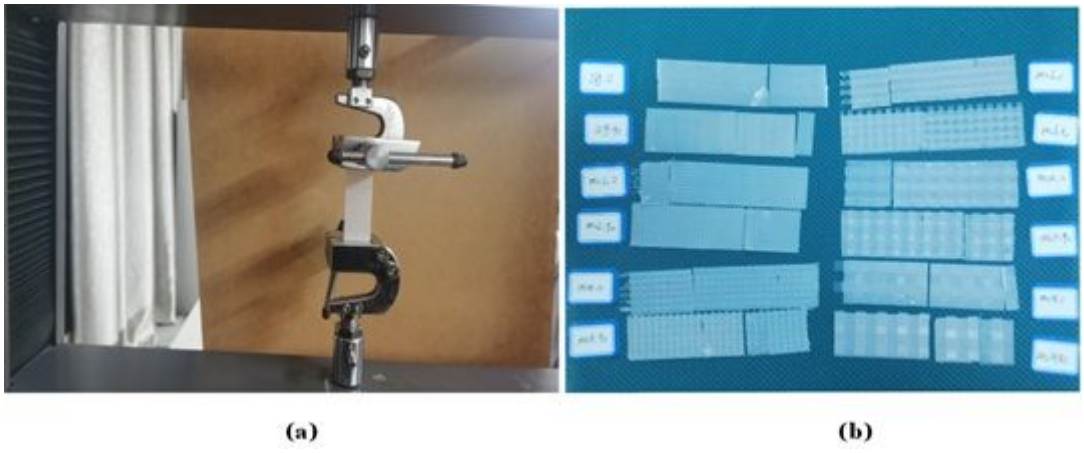

Figure 16

(a) Tensile properties test. (b) Twelve group of physical samples.

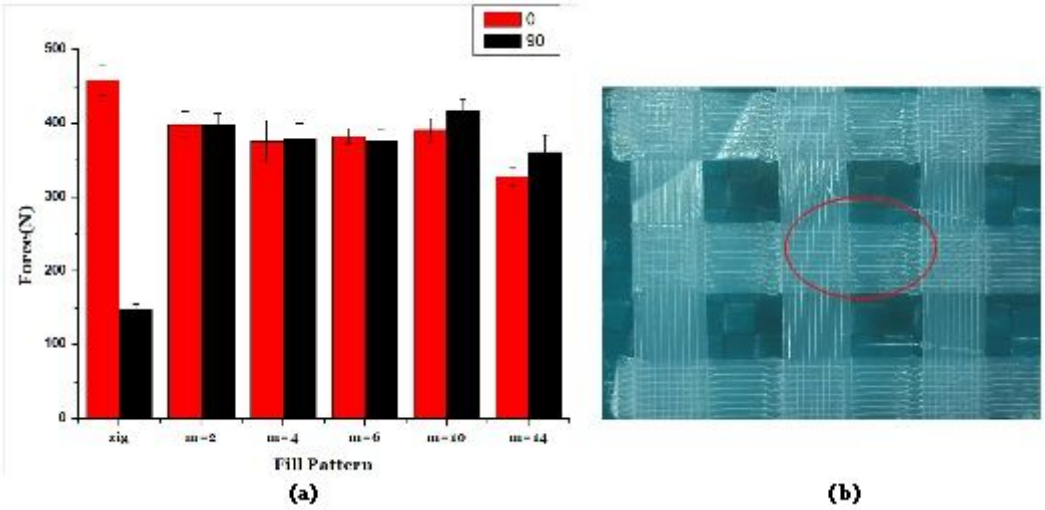

Figure 17

a) X-axis is filling pattern, Y-axis is the average of max force, red and black are double print direction which are orthorhombic. (b) When print nozzle up and down, the fusion material may be extruded or stretched in a split second

Supplementary Files

This is a list of supplementary files associated with this preprint. Click to download.

- Algorithm1.pdf